Performance characterizations and thermodynamic analysis of magnesium sulfate-impregnated zeolite 13X and activated alumina composite sorbents for thermal energy storage

S.Z. Xu [a,b], R.Z. Wang [a,*], L.W. Wang [a], J. Zhu [b]

[a] *Institute of Refrigeration and Cryogenics, Key Laboratory for Power Machinery and Engineering of M.O.E, Shanghai Jiao Tong University, 800 Dongchuan Road, Shanghai 200240, PR China*

[b] *Department of Architecture and Built Environment, University of Nottingham, University Park, Nottingham NG7 2RD, United Kingdom*

* Corresponding author. Tel./fax: +86 21 3420 6548.

E-mail addresses: zhizhi@sjtu.edu.cn (S.Z. Xu); rzwang@sjtu.edu.cn (R.Z. Wang); lwwang@sjtu.edu.cn (L.W. Wang); jie.zhu@nottingham.ac.uk (J. Zhu).

ABSTRACT

The composite sorbents of $MgSO_4$-impregnated zeolite 13X and activated alumina are developed for thermal energy storage (TES) with different temperature ranges. The sorption and desorption characteristics of raw and $MgSO_4$-impregnated activated alumina are studied, and the performances of the selected sorbents are tested in a closed-system TES device. The results are compared with those of raw and $MgSO_4$-impregnated zeolite 13X. It is shown that the impregnated $MgSO_4$ improves the overall TES performances of zeolite 13X and activated alumina. Compared to the raw host matrices, the impregnated $MgSO_4$ remarkably accelerates the temperature-rising rate of zeolite 13X to about three times and improves the temperature lift of activated alumina by 32.5%. The experimental energy storage densities of $MgSO_4$-impregnated zeolite 13X and activated alumina are 123.4 kWh $m^{-3}$and 82.6 kWh m^{-3}, respectively. The sorption temperature region of activated alumina is more aligned with the preferred hydration temperature of $MgSO_4$ in comparison with zeolite 13X. The hydration characteristics of $MgSO_4$ can resolve the solution leakage issue of open systems. Thermodynamic analysis is conducted to evaluate the performances of the TES device with different sorbents. It is found that entransy can be used to assess thermally and electrically driven TES systems reasonably.

Keywords: Sorption thermal energy storage; Thermochemical; Magnesium sulfate; Composite salt in porous matrix; Thermodynamic analysis.

Nomenclature

c_p	specific heat capacity at constant pressure [J kg^{-1}K^{-1}]
$E_{\mathrm{n,l}}$	entransy loss [J K]
$E_{\mathrm{x,d}}$	exergy destruction [J K^{-1}]
ESC	specific energy storage capacity [J kg^{-1}, Wh kg^{-1}]
ESD	energy storage density [J m^{-3}, kWh m^{-3}]
m	mass [kg]
$\dot{m}$	mass flow rate [kg s^{-1}]
p	pressure [Pa]
Q	heat [J]
q	heat flow [W]
T	temperature [K, °C]
$u(y)$	uncertainty of the quantity y
$u_{\mathrm{r}}(y)$	relative uncertainty of the quantity y
V	volume [m^3]
W	work (electrical) [J]
x	water uptake, adsorption ratio [g g^{-1}]

Greek letters

ΔT_{A}	temperature lift during sorption process [K]
$\delta z_{\max}$	maximum error of the quantity z
ε	exergy efficiency
η	energy efficiency
τ	time [s, h]
ξ	entransy efficiency

Subscripts

A	adsorption/sorption, adsorber
a	adsorbent/sorbent
C	condensing, condensation
chg	charging

D	desorption, dehydration
dis	discharging
E	evaporating, evaporation
eh	electric heater
f	fluid, flowing water
max	maximum
R	reservoir
S	sensible heat
sat	saturation

Superscripts

*	normalized

1. Introduction

With the development and modernization of civilization, thermal comfort has become essential in daily life. The pervasiveness of heating, ventilation, and air-conditioning (HVAC) systems in residential and commercial buildings improves the indoor thermal environment that people experience and makes the thermal exposures closer to the ideal conditions [1]. Buildings consume 35% of the world energy use and account for around one-third of the global CO_2 emissions [2]. In China, space and water heating is responsible for 71% of the final energy consumption in the residential sector and 68% of the final energy consumption in the commercial sector. In the European Union, 70% of the building final energy consumption is used for space and water heating, dominated by the residential space heating demand [2]. In the United Kingdom, direct gas use accounts for as high as 81% of the residential heat consumption for space and water heating, and electricity only delivers 8% [3]. Consequently, the transformation of heat sources from unsustainable fuels to renewable energy is crucial to mitigate the depletion of fossil fuels and solve energy crisis.

Solar thermal energy and renewable electricity are the most promising low-carbon heat sources substituting for fossil fuels. Thermal energy storage (TES) systems can alleviate or eliminate the discordance in time and power between heat supply and demand [4]. Therefore, solar heating systems with seasonal TES can substantially fulfill the heat demand and effectively reduce the heating peak in winter. Besides, with the increasing trend in renewable energy, electricity will become a utility source of sustainable energy in the coming decades, and electricity-to-heat systems comprising resistive heating and heat pumps will also become

low-carbon solutions for heating [5]. TES and electricity-to-heat are identified as effective measures to increase the flexibility of building energy systems [6]. Additionally, TES systems can also be charged by off-peak and excess electricity, which can improve the pattern and magnitude of electricity consumption [7].

Among all TES technologies, thermochemical heat storage, including sorption and chemical reaction, enjoys the highest energy storage density compared with sensible and latent heat storage [8]. Energy can be stored in the thermochemical TES medium at near ambient temperature without self-discharge. During the discharging process, the thermochemical TES medium experiences a noticeable temperature lift. These are essential features to realize long-term and seasonal TES [9]. Therefore, thermochemical TES systems allow more compact and longer-term storage of heat.

Magnesium sulfate ($MgSO_4$) is considered a promising thermochemical TES medium due to its high theoretical TES capability. The theoretical specific energy storage capacity of $MgSO_4$ is 3377 kJ kg^{-1}, and the theoretical energy storage density of its heptahydrate $MgSO_4 \cdot 7H_2O$ is 770 kWh m^{-3} [10]. However, it was reported that the real thermochemical performance of pure $MgSO_4$ is not ideal. For example, Bales et al. [11] found that energy storage density of $MgSO_4 \cdot 7H_2O$ descends to 420 kWh m^{-3} under suitable conditions. Van Essen et al. [12] tested a reactor with 40 g $MgSO_4$ under 150 °C charging temperature, 25 °C reactor temperature, and 25 °C evaporating temperature. They reported that the temperature lift in the hydration process of $MgSO_4$ is only about 6.5 °C. During the hydration process, the salt crystals may clump together and form a hardly permeable layer that impedes the water uptake [12, 13]. The kinetic hindrance prevents the material to display its full theoretical TES capability. The impregnation of the salt into host matrices and physical adsorbents is a measure to disperse the salt and solve the kinetic hindrance to the hydration reaction [13-15]. Meanwhile, the overall performance of the physical adsorbents also can be improved by the salt. Such a kind of materials is called composite salt in porous matrix (CSPM) [16].

Different porous materials have been used as the host matrix of $MgSO_4$ to produce CSPM materials for TES. Hongois et al. [17] first studied the characterization of the zeolite 13X/$MgSO_4$ composite with the salt mass fractions of 10%, 15%, and 20% for TES. They found that the optimum mass fraction of $MgSO_4$ is 15%, and the impregnation of $MgSO_4$ realizes an increase of 27% in the energy storage density compared to pure zeolite 13X. Xu et al. [18] tested the $MgSO_4$-impregnated zeolite 13X, 3A, and 4A composites. Their experimental results showed that the maximum water uptake of zeolite 13X/$MgSO_4$ impregnated in the solution with 20% salt mass fraction is 40% higher than that of pure zeolite 13X. Posern and Osburg [15] improved the temperature lift of $MgSO_4$ by 11–18 °C through impregnating the salt into activated carbon pellets. Brancato et al. [19] studied the $MgSO_4 \cdot 7H_2O$-embedded polymeric foams with salt hydrate mass fractions from 40% to 70%. They found that the threshold mass fraction around 60% realizes a good

compromise between the ability, flexibility, and hydration/dehydration capacity of the foam. Posern et al. [14] investigated the thermochemical characterizations of $MgSO_4$-impregnated porous glasses with different pore sizes. They concluded that CSPM materials are promising for thermochemical heat storage with high storage density. However, there are also negative results published in the literature. Whiting et al. [20] reported that the overall released heat of the zeolite Na-X/$MgSO_4$ composites with salt mass fractions of 5%, 10%, and 15% is significantly lower than that of zeolite Na-X. Mahon et al. [21] tested the characterizations of the zeolite 13X/$MgSO_4$ composites prepared by wetness impregnation and pellet press methods, but the dehydration peak of $MgSO_4$ was not observed for the samples. Given the different voices on the TES performance of $MgSO_4$-impregnated zeolite 13X, Xu et al. [10] investigated the characterizations of the zeolite 13X/$MgSO_4$ composite with the salt mass fraction of 15%. The results indicated that the impregnation of $MgSO_4$ remarkably accelerates the temperature-rising rate of the material in the sorption process, but the maximum water uptakes, temperature lifts, and specific energy storage capacities of zeolite 13X and zeolite 13X/$MgSO_4$ are similar.

In previous studies, $MgSO_4$ is generally considered to be a kind of mid-temperature salts with the discharging temperature of about 100 °C due to its dehydration temperature around 150 °C. As a result, $MgSO_4$ is usually impregnated into physical adsorbents with charging temperatures higher than 150 °C, such as zeolites. These physical adsorbents mostly have relatively high temperature lifts and adsorption heat. Nonetheless, the temperature lifts of $MgSO_4$ and $MgSO_4 \cdot H_2O$ measured under suitable conditions are very low, which indicates that the hydration reaction of $MgSO_4$ and its hydrates tends to slow down or even stop at the measured maximum hydration temperatures of 30–54 °C [12, 15, 22]. Therefore, hydration of the impregnated $MgSO_4$ can be severely hindered if the temperature lift of the host matrix is too high. Heretofore, although the discharging temperature, dehydration heat, hydration heat, pore size, and salt mass faction have been commonly referred to when selecting the TES medium and estimating the performance of the material [14, 17, 20, 21], the temperature lift and maximum sorption temperature have not been regarded as the influencing factors of the effect of the impregnated $MgSO_4$ in host matrices. Xu et al. [10] suggested that $MgSO_4$ should be impregnated into host matrices with lower temperature lifts and used for low-temperature TES with the discharging temperature much lower than 100 °C to alleviate the kinetic issue in the hydration reaction. The research objectives of this study are to develop CSPM materials with $MgSO_4$ for long-term TES with different temperature ranges and to show the impact of temperature lifts of host matrices on the performances of $MgSO_4$-impregnated sorbents.

In this study, zeolite 13X and activated alumina are selected as the host matrices of $MgSO_4$ for mid-temperature and low-temperature TES, respectively. The material characterizations of raw and $MgSO_4$-impregnated zeolite 13X and activated alumina are studied, and the TES performances of selected sorbents are

tested in a TES device. Thermodynamic analysis is conducted to evaluate the performances of the TES device with different sorbents. The results show that the impregnated $MgSO_4$ improves the overall TES performances of both zeolite 13X and activated alumina, and the improvement manners differ for host matrices with distinct temperature lifts.

2. Materials

In order to cover both mid-temperature and low-temperature TES, two kinds of physical adsorbents are selected as the host matrices for $MgSO_4$.

2.1. Host matrices

Zeolite 13X is an excellent physical adsorbent for TES because of its high adsorption heat, water uptake, and energy storage density [23]. Zeolite 13X–water TES systems generally enjoy high temperature lifts and good performances for mid-temperature heat storage as well as space and water heating [24-26]. Besides, zeolite 13X has been used as the host matrix for $MgSO_4$ to produce CSPM materials [10, 17, 18, 20, 21]. It was reported that $MgSO_4$-impregnated zeolite 13X with the salt mass fraction of 15% improves the energy storage density of zeolite 13X by approximately 15%–27% [10, 17]. The composite sorbent of zeolite 13X/$MgSO_4$ is suitable for mid-temperature TES, as its maximum sorption temperature is as high as 92–110 °C for long-term cycle [10]. Nonetheless, the high maximum sorption temperature of zeolite 13X does not match the preferred hydration condition of $MgSO_4$. The TES capability of $MgSO_4$ can be better utilized if it is impregnated into host matrices with relatively lower temperature lifts.

For low-temperature TES, silica gel, activated carbon, vermiculite, activated alumina, and expanded natural graphite are the promising host matrices [8]. Silica gel has been impregnated with LiCl [27], $CaCl_2$ [28], and $SrBr_2$ [29] to produce CSPM materials for low-temperature TES, and the energy storage densities range from 164 kWh m^{-3} to 203 kWh m^{-3} under the sorption temperatures of 30–35 °C and the charging temperature of 80 °C. Nonetheless, a pilot system with the silica gel–water working pair has the energy storage density of 50 kWh m^{-3}, which is only 25% of the theoretical value of silica gel, because of the limitations of the available heat source and sink [30]. Besides, silica gel loses its adsorption capability if the desorption temperature is higher than 120 °C [31], so the charging temperature must be strictly controlled. The activated carbon/$MgSO_4$ materials successfully improve the maximum hydration temperature of $MgSO_4$ by 11–18 °C in an open TES system, and the specific energy storage capacities are 1030–1270 kJ kg^{-1} [15]. However, carbon adsorbents do not have the preference for adsorption of water, which means that the impurities in the polluted air can displace water vapor from activated carbon in open systems [23]. The vermiculite composite sorbents

impregnated with $SrBr_2$ [32] and LiCl [33] have the predicted energy storage densities of 105 kWh m^{-3} and 224 kWh m^{-3}, respectively. The experimental study of an open TES system shows that vermiculite/$CaCl_2$ is a promising material for low-temperature heat storage with the energy storage density of 120–160 kWh m^{-3}, but vermiculite/$MgSO_4$ underperforms compared with the data on dehydration heat [34]. Activated alumina is a promising host matrix adsorbent for low-temperature TES because of its relatively high thermal conductivity and material strength. The LiCl-impregnated activated alumina has the predicted energy storage density of 318 kWh m^{-3} at 120 °C charging temperature [35]. An open sorption TES system with the activated alumina/LiCl composite sorbent realizes the energy storage density of 191 kWh m^{-3} for space heating [36]. Expanded natural graphite treated with sulfuric acid (ENG-TSA) has the advantage of high thermal conductivity. The ENG-TSA/$SrBr_2$ composite material significantly improves the heat transfer performance of $SrBr_2$, and the host matrix of ENG-TSA does not influence the water uptake of the material [29]. ENG-TSA is used as the host matrix for $MnCl_2$/$CaCl_2$ multi-salt sorbent for ammonia sorption, which enhances the heat and mass transfer performance of the composite sorbent [37, 38].

Zeolite 13X is suitable for mid-temperature TES with the maximum adsorption temperature higher than 90 °C, and activated alumina adapts to low-temperature TES below 60 °C. Both of these two host matrices have good water uptake performances and display potential for CSPM materials impregnated with $MgSO_4$. Besides, ENG-TSA is selected as the packing material to fill the gaps between the host matrix pellets. All the chosen materials can tolerate the high temperature of 300 °C, which simplifies the control of the sorbent temperature when the TES device is charged by the electric heater. As a result, in this study, zeolite 13X and activated alumina are selected as the host matrices of $MgSO_4$, and ENG-TSA is used as the packing material to increase the thermal conductivity when the sorbents are filled in the adsorber.

2.2. Composite sorbents

Figure 1 illustrates the preparation procedure of the composite sorbents [10]. First, the spherical host matrix pellets are dried in the oven (1). Then an appropriate amount of $MgSO_4$ aqueous solution is added to the host matrix pellets (2). The mixture is stirred and let stand for a long time to impregnate the salt into the host matrix (3). The impregnated salt content primarily depends on the concentration of the solution. Afterward, the pellets are taken out from the solution and dried again to remove water (4). The $MgSO_4$-impregnated host matrix is thus prepared. For the sorbents tested in the TES device, ENG-TSA is added as the packing material (5). The mixture is stirred until the constituents are uniformly distributed (6). The host matrix/$MgSO_4$/ENG-TSA composite is filled into the adsorber with the help of a mold (7). Finally, the material is compressed to let the pellets stack closely with ENG-TSA filling the clearance (8). For the host matrix/ENG-TSA sorbents

without $MgSO_4$, the preparation follows steps (1) and (5)–(8) in Figure 1.

According to Reference [17], the recommended mass fraction of magnesium sulfate for zeolite 13X/$MgSO_4$ is 15%, so the $MgSO_4$-impregnated zeolite 13X with the salt mass fraction of 15% (denoted as XM15) is prepared. The optimum salt mass fraction for activated alumina/$MgSO_4$ needs to be determined by material characterizations. Too high salt content can cause severer pore-blocking effect of the porous matrix, and too low salt content cannot provide adequate performance improvement of the composite sorbent. Therefore, $MgSO_4$-impregnated activated alumina sorbents with different salt contents are prepared for investigation.

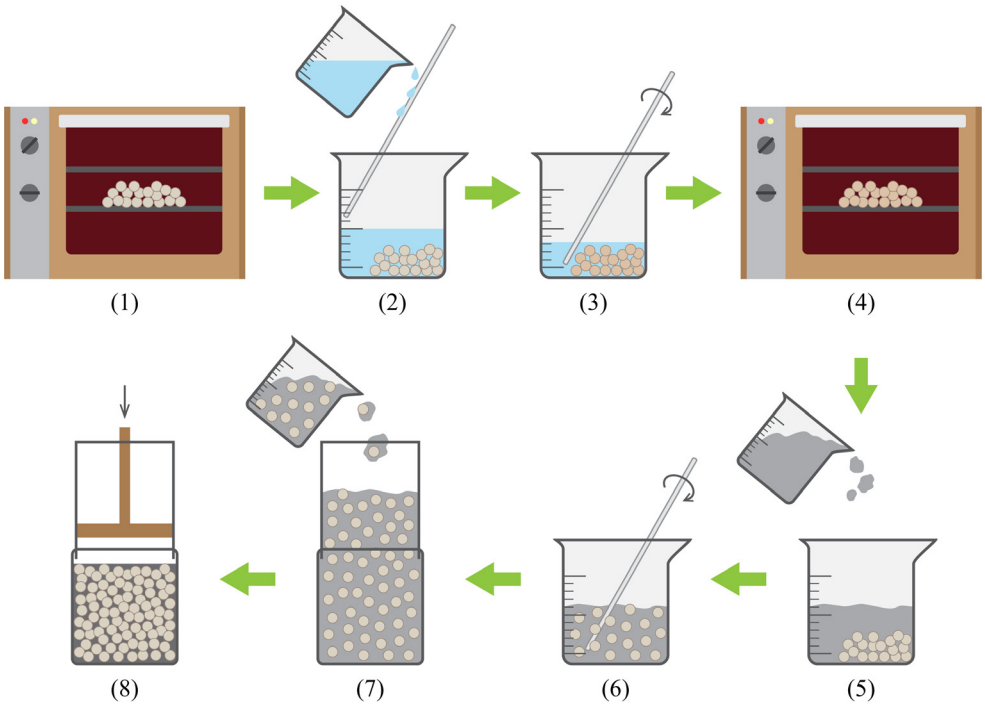

Figure 1. Preparation procedure of the sorbents.

Table 1 briefs the average constituent contents in the $MgSO_4$-impregnated activated alumina samples with different $MgSO_4$ solution concentrations.

Table 1. Contents in the $MgSO_4$-impregnated activated alumina samples.

Mass fraction of $MgSO_4$ in solution	4.75%	9.05%	13.0%	16.5%	20.4%
Mass fraction of $MgSO_4$ in sorbent	8.4%	11.1%	13.9%	16.5%	20.9%
Sorbent denoted as	AM8.4	AM11.1	AM13.9	AM16.5	AM20.9

3. Experimental methods

The performance characterizations of the sorbents are acquired from the material test and system experiments. The sorption and desorption characteristics of the sorbent samples are tested, and a TES device is applied to study the actual performances of the sorbents.

3.1. Material test

The sorption characteristics are described by the water uptake kinetic characteristics, i.e., the water uptake of the sorbents as functions of time during the sorption processes under typical conditions, which are obtained by measurement of the mass evolution of the sorbent samples placed in the constant temperature and humidity chamber. The sorbent samples are dried before the measurement.

The desorption characteristics are depicted by the simultaneous thermal analysis (STA) results, including thermogravimetric analysis and differential scanning calorimetry (TGA/DSC), which are conducted by the simultaneous thermal analyzer Netzsch STA 449 F3. The analyzer synchronously measures the mass evolution and heat flow variation of the sorbent samples during the heating and desorption processes. Considering that it is generally not feasible to heat the sorbent in the adsorber at a meager rate in practical application, the heating rate for STA is set to 5 °C min^{-1} that accords with the practical condition of the heating and desorption process in the TES device. The sorbent samples are placed in the constant temperature and humidity chamber to take in water thoroughly before the test.

3.2. System and procedure

Figure 2 shows the photo and schematic diagram of the TES device [10].

As depicted in Figure 2a, the sorption TES device mainly consists of an adsorber, a condenser/evaporator, and a reservoir. Pipes with valves link the condenser/evaporator and the reservoir. Figure 2b illustrates the internal structure of the TES device. The adsorber and the condenser/evaporator are connected by flanges. The condenser/evaporator contains a water tray with a vapor channel in the middle. Coil pipes go through the adsorber and the condenser/evaporator respectively. Electric heaters are attached to the outer surfaces of the adsorber and the reservoir separately. The adsorber is filled with the sorbent where several mass transfer channels made of perforated pipes and wire mesh are reserved for vapor flow. The TES device is connected to the vacuum pump and evacuated in the vacuum condition through V3, and water is added into the reservoir through V4. All the valves are closed before the experiments.

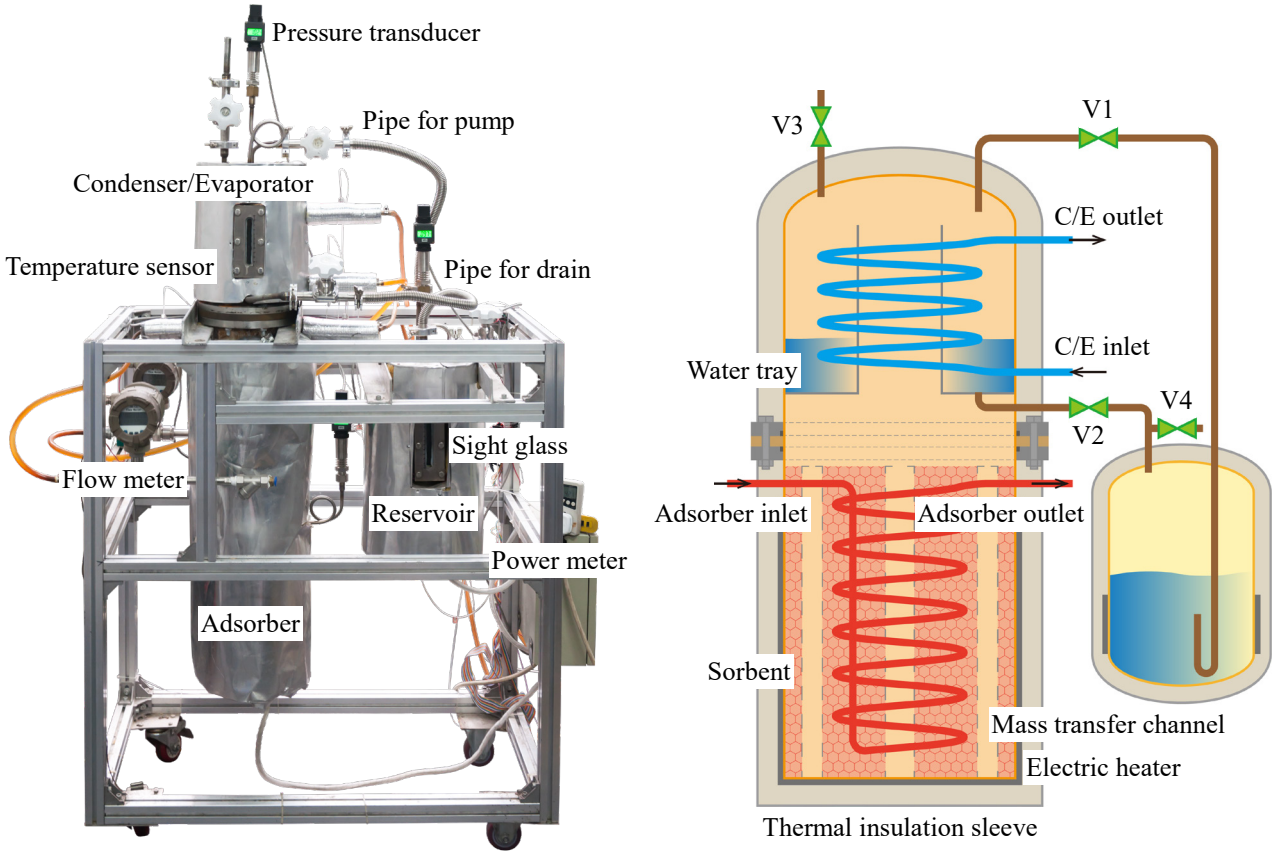

Figure 2. (a) Photo and (b) schematic diagram of the TES device.

The sorption TES device experiences two working phases in one cycle, i.e., the charging phase and the discharging phase [10]. During the charging phase, the adsorber electric heater is turned on to heat the sorbent, and water vapor is desorbed from the sorbent and condensed in the water tray of the condenser/evaporator. The fluid in the condenser/evaporator coil pipe is turned on which takes away the condensation heat. The adsorber electric heater is turned off when the sorbent temperature reaches the charging temperature, and the charging phase finishes. Afterward, V2 is opened to drain the water in the condenser/evaporator to the reservoir, and the fluid in the condenser/evaporator coil pipe is turned off. Then V2 is closed to separate the water in the reservoir from the sorbent in the adsorber, and thus self-discharging is avoided. During the discharging phase, the fluid in the adsorber coil pipe recovers the sensible heat from the sorbent. Before the sorption process starts, the fluid in the adsorber coil pipe is turned off. The reservoir electric heater is switched on to increase the temperature and pressure in the reservoir. When the vapor pressure in the reservoir is high enough to pump the water in the reservoir to the condenser/evaporator, the reservoir electric heater is switched off, and V1 is opened. After a sufficient amount of water is pumped, V1 is closed. The water evaporates from the water tray, and the water vapor is adsorbed by or reacts with the sorbent in the adsorber. The fluid in the condenser/evaporator

coil pipe is turned on to provide the evaporation heat. Sorption heat is released during the sorption process and elevates the temperature of the sorbent. When the sorbent temperature does not rise anymore, the fluid in the adsorber coil pipe is turned on to retrieve the sorption heat. The fluid in both coil pipes is turned off at the end of the discharging phase.

If the evaporating temperature is elevated, the TES device will operate as a sorption heat pump. In this case, a thermostatic bath is used to control the evaporating temperature of the system. When the evaporating temperature is above the room temperature, the fluid leaving the evaporator coil pipe is led to the adsorber coil pipe during the discharging phase so that the heat below the evaporating temperature will not be discharged.

4. Results

The sorbent samples of zeolite 13X (denoted as 13X), activated alumina (denoted as AA), $MgSO_4$-impregnated zeolite 13X (XM15) and $MgSO_4$-impregnated activated alumina (AM8.4, AM11.1, AM13.9, AM16.5, and AM20.9) are prepared. The sorbent characterizations of the prepared sorbents and the system performances of the selected sorbents are investigated.

4.1. Data processing

The specific desorption heat of the sorbent in STA is obtained by

$$Q_{\mathrm{D}}^{*} = -\frac{\Delta\tau}{m_{\mathrm{a,dry}}}\sum_{j=1}^{\frac{\tau}{\Delta\tau}} q_{\mathrm{D},j} \tag{1}$$

The heat measured in each process of the TES device is calculated by

$$Q_{\mathrm{S/A/C/E}} = \dot{m}_{\mathrm{f}} c_{p,\mathrm{f}} \Delta\tau \sum_{j=1}^{\frac{\tau}{\Delta\tau}} \left| T_{\mathrm{f,o}} - T_{\mathrm{f,i}} \right|_j \tag{2}$$

The temperature lift of the TES device during the sorption process is

$$\Delta T_{\mathrm{A}} = T_{\mathrm{A,max}} - T_{\mathrm{A}} \tag{3}$$

The specific energy storage capacity of the TES device is

$$\mathrm{ESC} = \frac{Q_{\mathrm{dis}}}{m_{\mathrm{a}}} = \frac{Q_{\mathrm{S}} + Q_{\mathrm{A}}}{m_{\mathrm{a}}} \tag{4}$$

The energy storage density of the TES device is

$$\mathrm{ESD} = \frac{Q_{\mathrm{dis}}}{V_{\mathrm{a}}} = \frac{Q_{\mathrm{S}} + Q_{\mathrm{A}}}{V_{\mathrm{a}}} \tag{5}$$

The statistical (type-A) uncertainty of the quantity z measured for n times is

$$u_{\mathrm{A}}(z)=\sqrt{\frac{1}{n(n-1)}\sum_{i=1}^{n}(z_i-\bar{z})^2} \tag{6}$$

The systematic (type-B) uncertainty of the quantity z directly measured by the instrument with a continuous uniform (rectangular) probability distribution is

$$u_{\mathrm{B}}(z)=\frac{\delta z_{\max}}{\sqrt{3}} \tag{7}$$

The combined uncertainty (type-A and type-B) of the quantity y is

$$u(y)=\sqrt{u_{\mathrm{A}}{}^2(y)+u_{\mathrm{B}}{}^2(y)} \tag{8}$$

The relative uncertainty of the indirectly-measured quantity y is calculated by

$$u_{\mathrm{r}}(y)=\frac{1}{y}\sqrt{\sum_j\left[\left(\frac{\partial y}{\partial z_j}\right)^2 u^2(z_j)\right]} \tag{9}$$

The calculated relative uncertainties of the discharging heat in the long-term TES cycles are approximately 11.4% for 13X/ENG-TSA, 9.1% for XM15/ENG-TSA, 8.7% for AA/ENG-TSA, and 6.3% for AM16.5/ENG-TSA.

4.2. Sorbent characterizations

Figure 3 presents the sorption characteristics of the raw zeolite 13X (13X), $MgSO_4$-impregnated zeolite 13X (XM15) [10], raw activated alumina (AA), and $MgSO_4$-impregnated activated alumina (AM8.4, AM11.1, AM13.9, AM16.5, and AM20.9) pellets. The sorbent samples are dried at 200 °C before the measurement.

As shown in Figure 3, most of the $MgSO_4$-impregnated composite sorbents display higher water uptake rates or amounts than those of the raw host matrixes. Raising the saturation temperature from 25 °C to 40 °C leads to significant improvement of the water uptake rates for all the tested sorbents. The water uptake amounts and rates of zeolite 13X sorbents (13X and XM15) are much higher than those of activated alumina sorbents (AA, AM8.4, AM11.1, AM13.9, AM16.5, and AM20.9). For example, under the saturation temperature of 25 °C, it requires approximately 1.2 hours for XM15 to reach the water uptake of 0.08 g g^{-1}, while AM16.5 needs more than 5 hours to get to the same water uptake.

In Figure 3a, the water uptake amounts of 13X under 25 °C and 40 °C saturation temperatures after 7 hours are 0.148 g g^{-1} and 0.160 g g^{-1}, respectively. The water uptake amounts of XM15 under 25 °C and 40 °C saturation temperatures after 7 hours are 0.156 g g^{-1} and 0.165 g g^{-1}, respectively. The impregnation of $MgSO_4$ in zeolite 13X improves the 7-hour water uptake amount and the water uptake rate slightly.

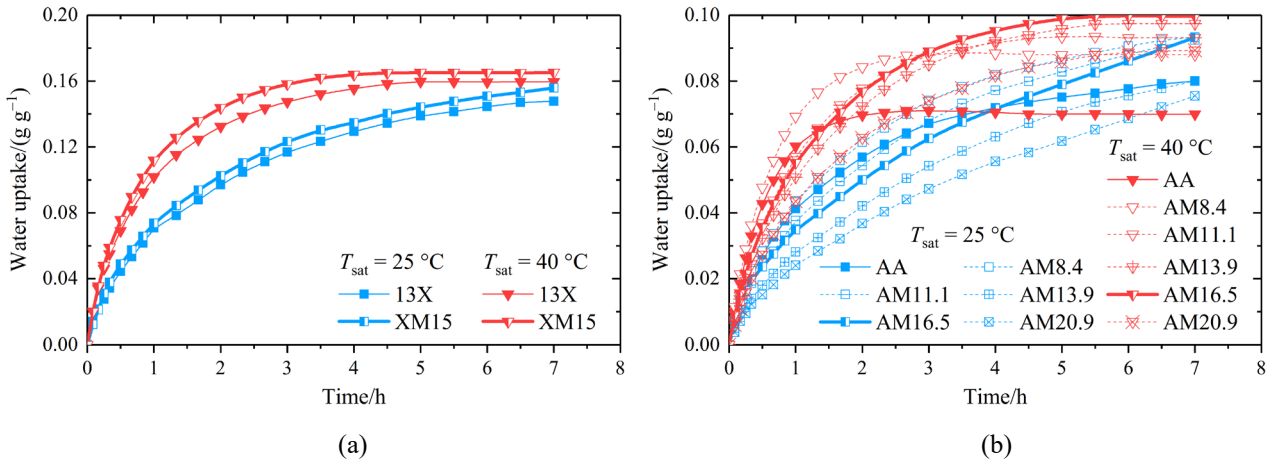

Figure 3. Sorption characteristics of the raw and $MgSO_4$-impregnated (a) zeolite 13X and (b) activated alumina pellets at the saturation temperatures of 25 °C and 40 °C.

According to Figure 3b, with the increase of the salt mass fraction for $MgSO_4$-impregnated activated alumina, the 7-hour water uptake amount and the water uptake rate tend to increase first and then decrease. Among all the $MgSO_4$-impregnated activated alumina sorbents, AM8.4 and AM16.5 have the highest 7-hour water uptake amounts under the saturation temperature of 25 °C, and AM16.5 has the highest 7-hour water uptake amount under 40 °C saturation temperature. AM20.9 has the lowest water uptake rate among all the activated alumina sorbents. Although AM8.6 shows a high water uptake rate, the 7-hour water uptake amount of AM8.6 under 40 °C saturation temperature is the lowest among the $MgSO_4$-impregnated activated alumina sorbents. As a result, according to the water uptake kinetic characteristics, AM16.5 displays the best overall performance among the $MgSO_4$-impregnated activated alumina sorbents. The 7-hour water uptake amounts of AA under the saturation temperatures of 25 °C and 40 °C are 0.080 g g^{-1} and 0.070 g g^{-1}, respectively. The 7-hour water uptake amounts of AM16.5 under 25 °C and 40 °C saturation temperatures are 0.093 g g^{-1} and 0.100 g g^{-1}, respectively.

Figure 4 illustrates the desorption characteristics of the raw zeolite 13X, $MgSO_4$-impregnated zeolite 13X [10], raw activated alumina, and $MgSO_4$-impregnated activated alumina pellets based on the STA results. The sorbent samples are put in the constant temperature and humidity chamber to take in water vapor thoroughly at 30 °C and 60% RH (relative humidity) before the test, which is a typical sorption condition for long-term closed-system TES.

As demonstrated in Figure 4, $MgSO_4$-impregnated zeolite 13X and activated alumina have higher maximum water uptake compared to the raw host matrixes. The maximum water uptake of XM15 is 0.01 g g^{-1} higher than that of 13X, and the maximum water uptakes of the $MgSO_4$-impregnated activated alumina sorbents are around 0.019 g g^{-1} higher than that of the raw activated alumina.

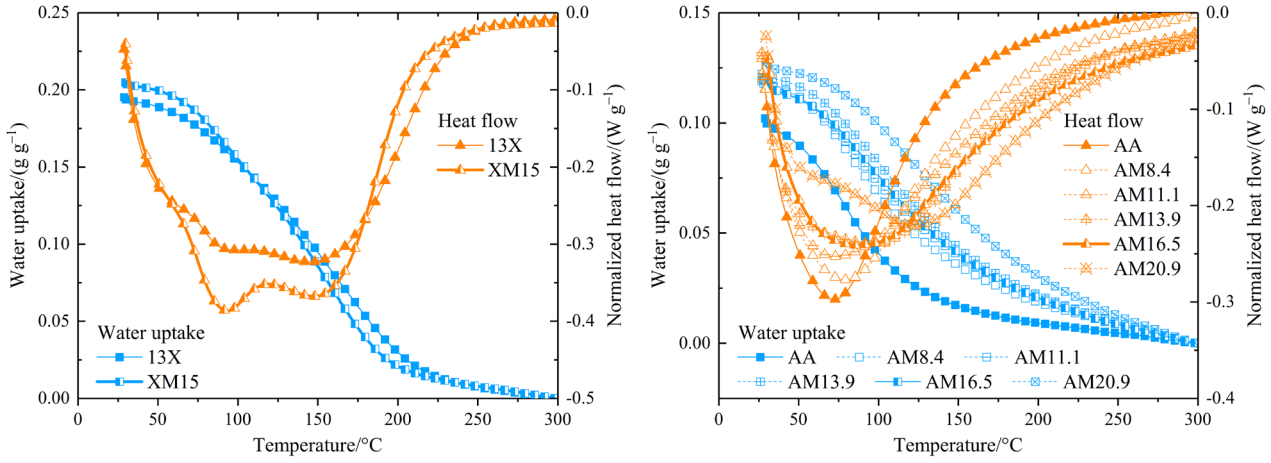

(a) (b)

Figure 4. Desorption characteristics of raw and $MgSO_4$-impregnated (a) zeolite 13X and (b) activated alumina pellets in the desorption processes.

The characteristics of the DSC curves for zeolite 13X and activated alumina sorbents are different. In Figure 4a, the DSC curve of 13X has only one endothermic peak during the heating and desorption process, whereas XM15 displays two endothermic peaks. The peak heat flow of XM15 is higher than that of 13X. In Figure 4b, with the increase of the salt mass fraction for $MgSO_4$-impregnated activated alumina, the endothermic peak has the general trend to descend towards the lower peak heat flow and to move right towards the higher temperature. All the activated alumina sorbents display only one endothermic peak individually. For XM15, the second endothermic peak mainly originates from the host matrix of zeolite 13X, and the first peak primarily results from the dehydration of $MgSO_4$ hydrates [10]. As for activated alumina, since the endothermic peak of $MgSO_4$ hydrates almost coincides with that of activated alumina, the $MgSO_4$-impregnated activated alumina sorbents each displays only one combined endothermic peak. Moreover, it can be seen that the pore-blocking effect in $MgSO_4$-impregnated activated alumina is severer than that in XM15, so the peak heat flow rises for zeolite 13X and descends for activated alumina after the impregnation of $MgSO_4$.

Table 2 outlines the STA results of the tested sorbents.

It can be found from Table 2 that the impregnated $MgSO_4$ improves the maximum water uptake and the specific desorption heat of zeolite 13X and activated alumina. The maximum water uptake and the specific desorption heat of XM15 are 5.1% and 6.3% higher than those of 13X, respectively. Although AM20.9 has the highest maximum water uptake after thorough sorption among all the $MgSO_4$-impregnated activated alumina sorbents, AM20.9 still contains the most amount of water uptake at the temperature of 200 °C. Thus AM20.9 has the lowest water uptake difference under the charging temperature of 200 °C. Among all the $MgSO_4$-

impregnated activated alumina sorbents, AM16.5 enjoys the highest specific desorption heat. The maximum water uptake and the specific desorption heat of AM16.5 are 15.7% and 35.7% higher than those of AA, respectively.

Table 2. STA results of raw and $MgSO_4$-impregnated zeolite 13X and activated alumina pellets.

Sorbent	Maximum water uptake/(g g^{-1})	Specific desorption heat/(kJ kg^{-1})	Peak heat flow/(W g^{-1})	Temperature at peak heat flow/°C
13X	0.195	598.25	−0.323	145.5
XM15	0.205	635.84	−0.386, −0.368	93.2, 147.9
AA	0.102	313.89	−0.297	71.7
AM8.4	0.119	375.90	−0.277	78.7
AM11.1	0.119	402.03	−0.253	71.4
AM13.9	0.122	415.23	−0.239	96.0
AM16.5	0.118	425.86	−0.241	85.6
AM20.9	0.126	420.43	−0.221	121.4

In summary, both the water uptake kinetic characteristics and the STA results indicate the better performances of the $MgSO_4$-impregnated zeolite 13X and activated alumina than raw host matrices. The recommended salt mass fraction for $MgSO_4$-impregnated zeolite 13X is 15% according to the literature [17], and the optimum salt content of $MgSO_4$-impregnated activated alumina is 16.5% based on the water uptake kinetic characteristics and STA results. Thus, XM15 and AM16.5 are adopted as the sorbents to be tested in the TES device, and 13X and AA are also tested for comparison.

4.3. System performances

The sorbents of 13X/ENG-TSA, XM15/ENG-TSA, AA/ENG-TSA, and AM16.5/ENG-TSA are filled into the adsorber of the TES device separately, and the system performances under different conditions are tested. The sorbents are heated to the discharging temperature and kept for hours when the TES device is evacuated in the vacuum condition for thorough desorption. According to the STA results in Figure 4, the discharging temperatures of 13X/ENG-TSA, XM15/ENG-TSA, AA/ENG-TSA, and AM16.5/ENG-TSA are set to 250 °C, 250 °C, 150 °C, and 200 °C, respectively. Figure 5a shows the evolution of sorbent temperatures of different types of well-regenerated sorbents during the sorption processes in the TES device, and Figure 5b presents the division of the discharging heat.

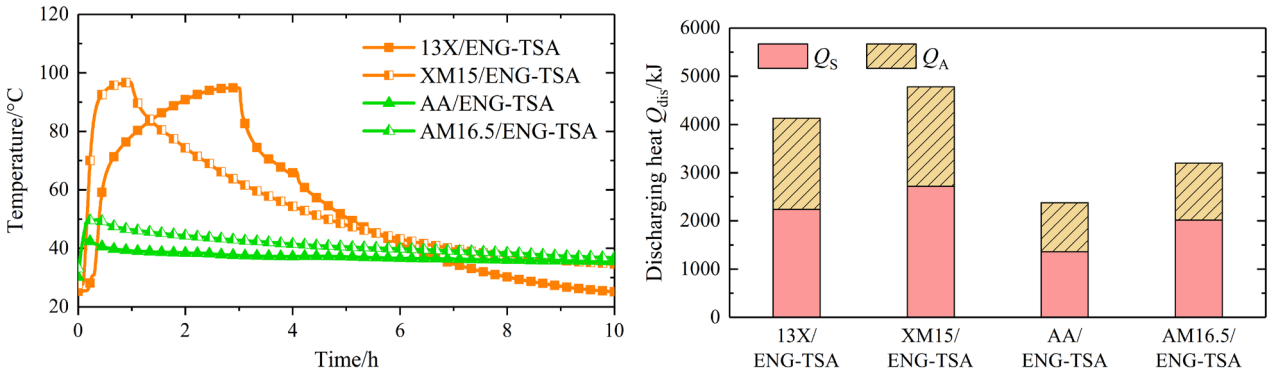

(a) (b)

Figure 5. (a) Evolution of sorbent temperatures of 13X/ENG-TSA, XM15/ENG-TSA, AA/ENG-TSA, and AM16.5/ENG-TSA during sorption processes in the TES device and (b) division of discharging heat.

As shown in Figure 5a, zeolite 13X sorbents (13X/ENG-TSA and XM15/ENG-TSA) have the dramatically higher maximum sorption temperatures and temperature lifts than those of activated alumina sorbents (AA/ENG-TSA and AM16.5/ENG-TSA). It can be found that 13X/ENG-TSA and XM15/ENG-TSA have the similar maximum sorption temperatures, whereas the temperature-rising rate of XM15/ENG-TSA is approximately three times of that of 13X/ENG-TSA. Compared to AA/ENG-TSA, AM16.5/ENG-TSA has the markedly higher maximum sorption temperature, but the temperature-rising rates of AA/ENG-TSA and AM16.5/ENG-TSA are similar.

From Figure 5b, the discharging heat of XM15/ENG-TSA and AM16.5/ENG-TSA are improved by about 14.7% and 34.9% compared with 13X/ENG-TSA and AA/ENG-TSA, respectively. The sorption heat is slightly increased after the impregnation of $MgSO_4$, and either the temperature-rising rate or the temperature lift of the material is notably elevated. In consequence, the impregnated $MgSO_4$ improves the overall TES performances of the zeolite 13X and activated alumina sorbents.

The performances of XM15/ENG-TSA and AM16.5/ENG-TSA are further tested in the TES device. If the evaporating temperature is raised, the maximum sorption temperature also can be elevated, and the TES device will operate as a sorption heat pump. Figure 6a shows the evolution of sorbent temperatures of XM15/ENG-TSA and AM16.5/ENG-TSA during the sorption processes in the TES device under 25 °C, 30 °C, and 40 °C evaporating temperatures, and Figure 6b illustrates the division of the discharging heat.

From Figure 6a it can be found that the maximum sorption temperatures and the temperature lifts of XM15/ENG-TSA and AM16.5/ENG-TSA rise with the increase of the evaporating temperature when the sorption temperature does not change. The variation of the maximum sorption temperature of XM15/ENG-

TSA with the evaporating temperature is much more significant than that of AM16.5/ENG-TSA.

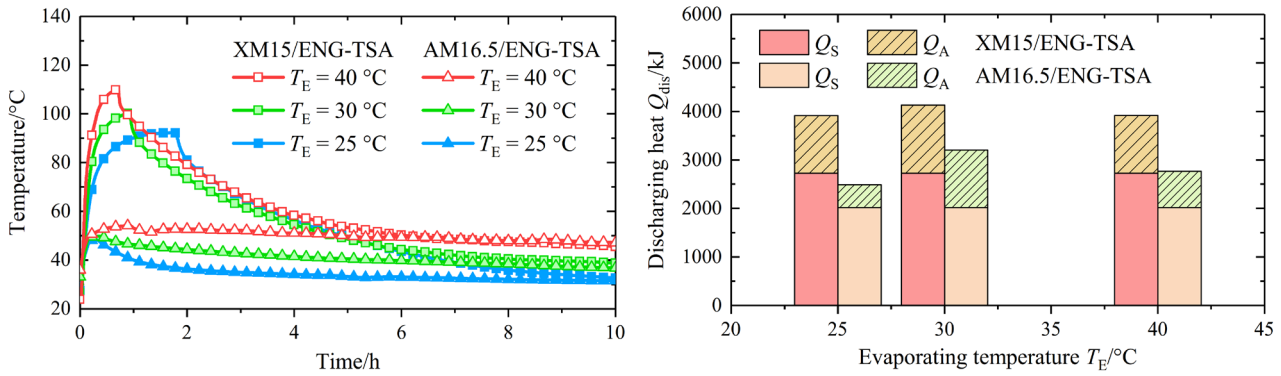

(a) (b)

Figure 6. (a) Evolution of sorbent temperatures of XM15/ENG-TSA and AM16.5/ENG-TSA during sorption processes in the TES device under 25 °C, 30 °C, and 40 °C evaporating temperatures and (b) division of discharging heat.

According to Figure 6b, the discharging heat of XM15/ENG-TSA and AM16.5/ENG-TSA at the evaporating temperature of 30 °C is higher compared to the other conditions. There are only minor differences among the discharging heat of XM15/ENG-TSA at different evaporating temperatures, but for AM16.5/ENG-TSA, the discharging heat at the evaporating temperature of 30 °C is noticeably higher than the other conditions. Although the high evaporating temperature can increase the pressure of water vapor and thus promote the water uptake rate, it affects the maximum water uptake and hinders the hydration of $MgSO_4$, as the sorbent temperature in the sorption process is also elevated. The evaporating temperature of 30 °C realizes the balance between the two effects. For XM15/ENG-TSA, since the temperature lift and the maximum sorption temperature are high enough, the evaporating temperature from 25 °C to 40 °C seemingly does not have much influence on the discharging heat. As for AM16.5/ENG-TSA, the maximum sorption temperature is in the range of 48–54 °C, which is much closer to the evaporating temperature range of 25–40 °C, so the influence of the evaporating temperature on the discharging heat is more noticeable compared with XM15/ENG-TSA.

If the sorption process is initiated before the sensible heat is completely retrieved, the sorption temperature will be higher than the ambient temperature, and the remaining sensible heat will be recovered along with the released sorption heat. This circumstance is for short-term TES. Figure 7a shows the variation of sorbent temperatures in the sorption processes with the composite sorbents of XM15/ENG-TSA and AM16.5/ENG-TSA under the sorption temperatures of 30 °C, 60 °C, and 80 °C, and Figure 7b shows the division of the discharging heat.

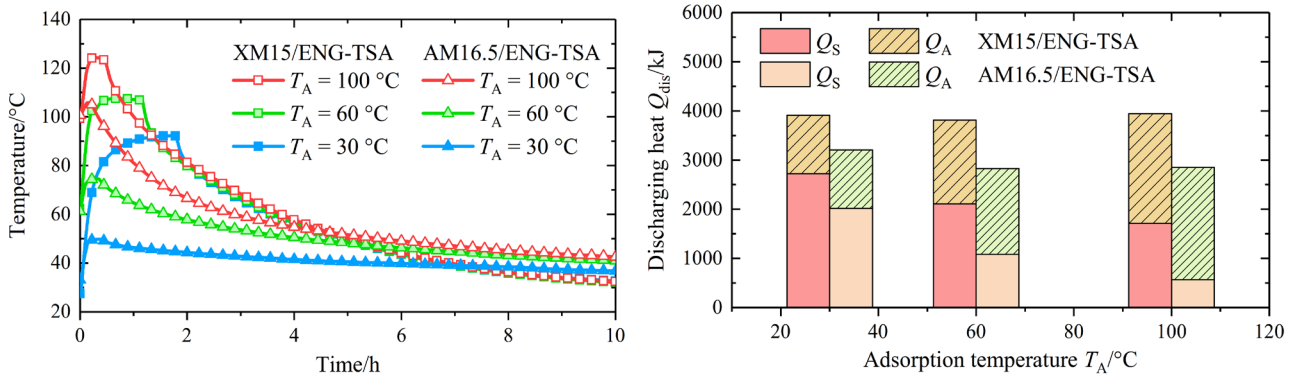

(a) (b)

Figure 7. (a) Evolution of sorbent temperatures of XM15/ENG-TSA and AM16.5/ENG-TSA during sorption processes in the TES device under 30 °C, 60 °C, and 80 °C sorption temperatures and (b) division of discharging heat.

According to Figure 7a, the maximum sorption temperatures of XM15/ENG-TSA and AM16.5/ENG-TSA increase with the rise of the sorption temperature, whereas the temperature lifts decrease with the increasing sorption temperature. The time for AM16.5/ENG-TSA to reach the maximum sorption temperature is similar under different sorption temperatures. However, for XM15/ENG-TSA, the lower the sorption temperature is, the much longer time the sorbent requires to get to the maximum sorption temperature. Although XM15/ENG-TSA needs longer time to reach the maximum sorption temperature compared to AM16.5/ENG-TSA, the temperature-rising rate and the temperature lift of XM15/ENG-TSA are all higher than those of AM16.5/ENG-TSA.

From Figure 7b, the discharging heat of XM15/ENG-TSA is similar under different sorption temperatures, whereas for AM16.5/ENG-TSA, the discharging heat at 30 °C evaporating temperature is markedly higher in comparison with the other conditions. The reason is that the sorption temperatures of 60 °C and 100 °C are beyond the preferred temperature range of activated alumina, and the high sorption temperature affects the discharging heat of AM16.5/ENG-TSA more severely than XM15/ENG-TSA. Compared with AM16.5/ENG-TSA, the higher temperature lift of XM15/ENG-TSA mainly benefits from the higher specific adsorption heat of zeolite 13X. Nevertheless, the sorption heat of XM15/ENG-TSA decreases a bit after several cycles, whereas AM16.5/ENG-TSA seemingly does not suffer from such detectable performance attenuation. This is because zeolite 13X can adsorb air as well and thus is more sensitive to the slight vacuum loss of the device compared to activated alumina. This problem can be solved by regenerating the sorbents in the vacuum condition or further decreasing the leak rate of the device.

Table 3 outlines the performance parameters of the TES device with different sorbents.

Table 3. Performance parameters of the TES device with different sorbents

Parameter	13X/ENG-TSA	XM15/ENG-TSA	AA/ENG-TSA	AM16.5/ENG-TSA
m_a/kg	7.245	8.465	7.508	8.920
ρ_a/(kg m^{-3})	673	786	697	828
T_{chg}/°C	250	250	150	200
T_{dis}/°C	25–90	25–90	30–70	30–70
W_{eh}/kJ	8323	9644	6686	7442
Q_{dis}/kJ	4131	4783	2374	3202
ΔT_A/°C	69.6	69.2	12.6	16.7
ESC/(Wh kg^{-1})	158.4	157.0	87.8	99.7
ESD/(kWh m^{-3})	106.5	123.4	61.2	82.6

5. Discussion

Thermodynamic analysis is conducted to evaluate the performances of the TES device with different sorbents. The effect of the impregnated $MgSO_4$ in the composite sorbents, the relevant influencing factors of the sorbent performances, and the applications of the sorbents are discussed.

5.1. Thermodynamic analysis

In addition to the performance parameters listed in Table 3, the thermodynamic evaluation indices of energy efficiency, exergy destruction, exergy efficiency, entransy loss, and entransy efficiency are studied.

The energy efficiency of the TES device depends on the useful heat output of the system. Typically, the useful heat includes sensible heat and sorption heat. For low-temperature TES, when the condensing temperature is high enough to provide heat output, condensation heat can be regarded as useful heat as well. For seasonal TES, sensible heat is dissipated to the ambient after prolonged storage time, and only sorption heat can be recovered to provide useful heat output. Therefore, considering the different usage scenario, three types of energy efficiency are analyzed.

The (typical) energy efficiency of the TES device is

$$\eta = \frac{Q_{dis}}{W_{eh}} = \frac{Q_S + Q_A}{W_{eh}} \tag{10}$$

The energy efficiency including condensation heat of the TES device is calculated by

$$\eta_{\mathrm{C+}} = \frac{Q_{\mathrm{S}} + Q_{\mathrm{A}} + Q_{\mathrm{C}}}{W_{\mathrm{eh}}} \tag{11}$$

The seasonal energy efficiency of the TES device is obtained by

$$\eta_{\mathrm{S-}} = \frac{Q_{\mathrm{A}}}{W_{\mathrm{eh}}} \tag{12}$$

The ideal seasonal energy efficiency of the TES device with compensation for heat loss of the electric heaters and the metal heat capacity can be calculated by

$$\eta_{Q,\mathrm{S-}} = \frac{Q_{\mathrm{A}}}{Q_{\mathrm{chg}}} = \frac{Q_{\mathrm{A}}}{\left(m_{\mathrm{a}} - m_{\mathrm{ENG\text{-}TSA}}\right) Q_{\mathrm{D}}^{*} + m_{\mathrm{ENG\text{-}TSA}} \int_{\mathrm{chg}} c_{p,\mathrm{ENG\text{-}TSA}} \mathrm{d}T_{\mathrm{a}}} \tag{13}$$

The exergy destruction of the TES device is obtained by

$$E_{\mathrm{x,d}} = W_{\mathrm{eh}} - \int_{\mathrm{S}} \left(1 - \frac{T_0}{T_{\mathrm{a}}}\right) \delta Q_{\mathrm{S}} - \int_{\mathrm{A}} \left(1 - \frac{T_0}{T_{\mathrm{a}}}\right) \delta Q_{\mathrm{A}} + \int_{\mathrm{E}} \left(\frac{T_0}{T_{\mathrm{E}}} - 1\right) \delta Q_{\mathrm{E}} - \int_{\mathrm{C}} \left(1 - \frac{T_0}{T_{\mathrm{C}}}\right) \delta Q_{\mathrm{C}} \tag{14}$$

The exergy efficiency of the TES device is calculated by

$$\varepsilon = \frac{\int_{\mathrm{S}} \left(1 - \frac{T_0}{T_{\mathrm{a}}}\right) \delta Q_{\mathrm{S}} + \int_{\mathrm{A}} \left(1 - \frac{T_0}{T_{\mathrm{a}}}\right) \delta Q_{\mathrm{A}}}{W_{\mathrm{eh}}} \tag{15}$$

The entransy loss of the TES device is defined as

$$E_{\mathrm{n,l}} = \int_{\mathrm{eh}} T \delta W_{\mathrm{eh}} - \int_{\mathrm{S}} T_{\mathrm{a}} \delta Q_{\mathrm{S}} - \int_{\mathrm{A}} T_{\mathrm{a}} \delta Q_{\mathrm{A}} + \int_{\mathrm{E}} T_{\mathrm{E}} \delta Q_{\mathrm{E}} - \int_{\mathrm{C}} T_{\mathrm{C}} \delta Q_{\mathrm{C}} \tag{16}$$

The entransy efficiency of the TES device is defined as

$$\xi = \frac{\int_{\mathrm{S}} T_{\mathrm{a}} \delta Q_{\mathrm{S}} + \int_{\mathrm{A}} T_{\mathrm{a}} \delta Q_{\mathrm{A}}}{\int_{\mathrm{eh}} T \delta W_{\mathrm{eh}}} \tag{17}$$

The aforementioned thermodynamic evaluation indices of the TES device with different sorbents are summarized in Table 4.

According to Table 4, the energy efficiency of activated alumina sorbents (AA/ENG-TSA and AM16.5/ENG-TSA) is lower than that of zeolite 13X sorbents (13X/ENG-TSA and XM15/ENG-TSA) because activated alumina sorbents have the slower water uptake kinetic characteristics and experience longer cycles. Nevertheless, the energy efficiency including condensation heat of AM16.5/ENG-TSA is as high as 0.712. Although the ideal seasonal energy efficiency of AA/ENG-TSA is the highest among the tested sorbents, the real seasonal energy efficiency of AA/ENG-TSA decreases significantly. The reason is that the charging heat of AA/ENG-TSA is the lowest among the tested sorbents, but meanwhile, the proportion of the electricity input of the reservoir electric heater used to pump water is the highest, and the long cycle time of activated alumina sorbents causes more heat dissipation. The actual energy efficiency can be raised if the thermal

insulation is improved, the heat and mass transfer is enhanced, and the energy storage capacity of the system is increased. Besides, the ideal energy efficiency of $MgSO_4$-impregnated sorbents tends to be lower than that of raw host matrices, as the additional desorption heat of $MgSO_4$ hydrates cannot provide enough increase of the hydration heat. Consequently, in practical application, if the water uptake rate during the later period of the sorption process becomes too slow to provide effective discharging heat power, the further water uptake can be excess and should be avoided to reduce the required charging heat and improve the energy efficiency, especially for $MgSO_4$-impregnated sorbents.

Table 4. Thermodynamic analysis of the TES device with different sorbents

Parameter	13X/ENG-TSA	XM15/ENG-TSA	AA/ENG-TSA	AM16.5/ENG-TSA
η	0.496	0.496	0.355	0.430
η_{C+}	0.666	0.667	0.565	0.712
η_{S-}	0.227	0.214	0.151	0.159
$\eta_{Q,S-}$	0.450	0.399	0.502	0.379
$E_{x,d}$/kJ	7766	8839	6484	7094
ε	0.0624	0.0886	0.0260	0.0406
$E_{n,l}$/(MJ K)	2085	2376	1594	1777
ξ	0.433	0.456	0.326	0.380

Entropy, exergy, and entransy have been used to analyze the adsorption system [39], cascaded latent heat storage system [40], and thermochemical heat storage reactor [41], but the essential distinctions, applicable occasions, and optimization objectives of these thermodynamic evaluation indicators still seem vague in the previous studies. It is known that entransy dissipation and entropy production are both irreversibility-directing concepts, so they both can be used to analyze heat exchange processes without heat–work interaction and give the same direction of optimization, i.e., to decrease the irreversibility [42]. Nevertheless, since the definitions and physical meanings of entropy and entransy are different, the detailed optimum results with respect to them can be different.

As electrically driven TES systems charged by off-peak and excess electricity can deliver high flexibility and improve the electricity consumption profile, thermodynamic assessment should cover both thermally and electrically driven TES systems and exhibit enough comparability between the two kinds of TES systems. However, it is evident that exergy destruction of electrically driven TES systems is distinctively higher than that of thermally driven TES systems because of the severe exergy loss in the electricity-to-heat conversion.

On the contrary, based on the theory of entransy, the entransy transfer accompanied with work transfer has the same form with heat transfer, as indicated in Equation (18). As a result, entransy provides the possibility of assessing thermally and electrically driven TES systems reasonably with the identical thermodynamic evaluation index.

$$\delta Q = \mathrm{d}U + \delta W \Rightarrow T\delta Q = T\mathrm{d}U + T\delta W \tag{18}$$

From Table 4, it can be found that the exergy efficiency of the TES device with the tested sorbents is only 0.026–0.089, which is much lower than the energy efficiency. Given that the electrically driven TES system is generally charged by off-peak and excess electricity, the useful thermal energy discharged by the TES system can be more valuable than the excess electricity used to charge the system. Consequently, it is not appropriate to assess electrically driven TES systems by exergy in some circumstances. The entransy efficiency of the TES device is in the range of 0.326–0.456, which is slightly lower than the energy efficiency due to the temperature degradation of the TES device. As a result, entransy can be used to assess thermally and electrically driven TES systems reasonably. Entransy loss and entransy efficiency are useful to assess the TES system especially when the exergy difference between charging heat and excess electricity is of marginal importance. For example, as utilization of excess renewable electricity is almost as environmentally friendly as recovery of waste heat, both of them will be considerable heating sources to charge the TES system.

5.2. Evaluation of sorbents

Figure 8 gives the comparison of the predicted, experimental, and theoretical energy storage densities of zeolite 13X, activated alumina, and $MgSO_4$ sorbents. The predicted energy storage densities are calculated based on the calorimetry results, the experimental energy storage densities are tested with the TES device, and the theoretical energy storage densities are calculated from the tested specific desorption heat of the host matrices and the reaction enthalpy of $MgSO_4$ and $MgSO_4 \cdot 7H_2O$.

From Figure 8 it can be found that the sorption heat measured with the TES device is comparable to the desorption heat obtained from the calorimetry results, but the composite sorbents do not display the full theoretical energy storage density of the impregnated $MgSO_4$. Although the theoretical energy storage density of $MgSO_4 \cdot 7H_2O$ calculated from the reaction enthalpy is as high as 770 kWh m^{-3}, the applicable energy storage densities of the composite sorbents are limited by the actual dehydration and hydration performances under practical conditions. Contrary to the ideal TES performances implied by the isothermal calorimetry results [15], the practical sorption and desorption conditions are not isothermal, and the materials should experience temperature lifts to provide useful discharging heat. Consequently, the TES capabilities of the materials are generally restricted by reaction kinetics as well as heat and mass transfer performances. Nevertheless, the

sorption heat is still closed to the desorption heat under practical conditions if adequate discharging time is permitted for reaction.

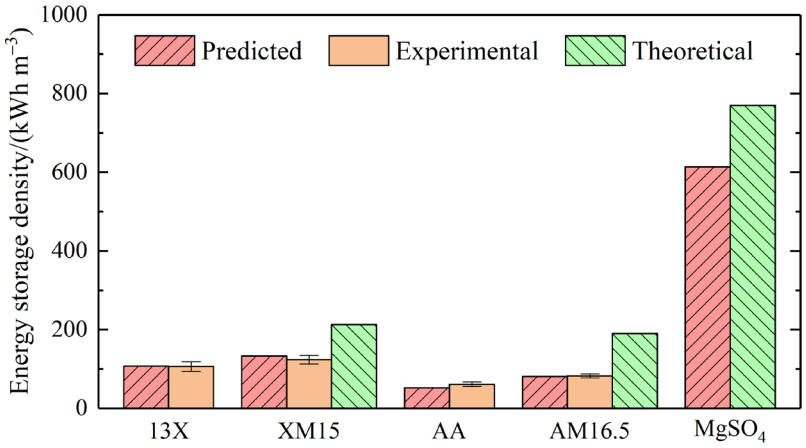

Figure 8. Comparison of the predicted, experimental, and theoretical energy storage densities of zeolite 13X, activated alumina, and $MgSO_4$ sorbents.

Figure 9 illustrates the relative humidity–temperature phase diagram of $MgSO_4$–H_2O system [10, 13] and the sorption condition regions of AM16.5 and XM16.5. The colored curves represent the saturation temperatures of 25 °C, 30 °C, 35 °C, and 40 °C. Curves a, b, and c are the deliquescence–crystallization equilibria of $MgSO_4 \cdot 7H_2O$, $MgSO_4 \cdot 6H_2O$, and $MgSO_4 \cdot H_2O$, respectively. Curves d, e, and f are the hydration–dehydration equilibria of $MgSO_4 \cdot 6H_2O$–$MgSO_4 \cdot 7H_2O$, $MgSO_4 \cdot H_2O$–$MgSO_4 \cdot 6H_2O$, and $MgSO_4 \cdot H_2O$–$MgSO_4 \cdot 7H_2O$, respectively. Curves g and h are the deliquescence curves of $MgSO_4 \cdot H_2O$ and $MgSO_4 \cdot 6H_2O$, respectively.

In order to achieve sufficient discharging heat in the sorption process, the advantaged sorption condition region of $MgSO_4$ lies above equilibria c, e, and f in Figure 9, where the temperature and relative humidity enable the hydration reaction of $MgSO_4 \cdot 7H_2O$ or $MgSO_4 \cdot 6H_2O$. According to the experimental results, the preferred evaporating temperatures of XM15 and AM16.5 are around 30 °C. The sorption condition regions of XM15 and AM16.5 are marked by the shaded area with diagonal lines in Figure 9. The maximum sorption temperatures of AM16.5 and XM15 are 49.8 °C and 96.8 °C, respectively. It can be seen that the sorption condition region of AM16.5 is mainly located above equilibria c, e, and f when the sorbent temperature is below about 40 °C, while the sorption condition region of XM15 mostly crosses equilibria e and extends to the kieserite region when the temperature is higher than approximately 40 °C. Therefore, the impregnated $MgSO_4$ in AM16.5 tends to form $MgSO_4 \cdot 7H_2O$ and $MgSO_4 \cdot 6H_2O$ in the major stages of the sorption process, whereas the impregnated $MgSO_4$ in XM15 can be hydrated to $MgSO_4 \cdot 7H_2O$ and $MgSO_4 \cdot 6H_2O$ only during

the early and late stages of the sorption process. Moreover, the high temperature lift of zeolite 13X may cause dehydration of $MgSO_4 \cdot 7H_2O$ and $MgSO_4 \cdot 6H_2O$ during the sorption process, which consumes some of the sorption heat released at high sorbent temperature. As a result, the sorption temperature region of activated alumina is more aligned with the preferred hydration temperature of $MgSO_4$ in comparison with zeolite 13X.

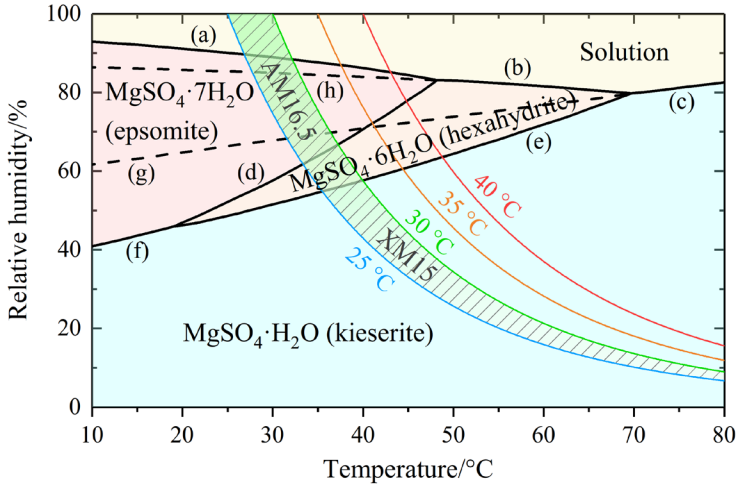

Figure 9. Relative humidity–temperature phase diagram of $MgSO_4$–H_2O system and sorption condition regions of AM16.5 and XM15.

The different temperature lifts of the host matrices result in the distinct improvement manners of the $MgSO_4$-impregnated sorbents. Compared to the raw host matrices, the impregnated $MgSO_4$ remarkably accelerates the temperature-rising rate of zeolite 13X to about three times and improves the temperature lift of activated alumina by 32.5%. The reason is that the high temperature lift of zeolite 13X impedes the persistent hydration of $MgSO_4$, and the initial hydration heat of $MgSO_4$ and its hydrates at low sorbent temperature still contributes to the temperature-rising rate of the composite sorbent. As for activated alumina, the temperature lift of the host matrix is low, and thus it will not interfere with the hydration of $MgSO_4$ and the release of hydration heat. The sorption heat of $MgSO_4$-impregnated zeolite 13X and activated alumina is increased by 8.8% and 17.2%, respectively, in comparison with the raw host matrices. The energy efficiency of $MgSO_4$-impregnated activated alumina is notably higher than that of activated alumina, but the energy efficiency of $MgSO_4$-impregnated zeolite 13X is similar to that of zeolite 13X, and the seasonal efficiency of raw and $MgSO_4$-impregnated host matrices is similar. Although the entransy loss of $MgSO_4$-impregnated zeolite 13X and activated alumina is higher than that of raw host matrices, the entransy efficiency of $MgSO_4$-impregnated zeolite 13X and activated alumina is noticeably higher than that of raw host matrices, which implies that the impregnated $MgSO_4$ improves the mean discharging temperatures of the sorbents.

The pore sizes of zeolite 13X [17] and activated alumina [35] are around 0.8–0.9 nm and 1.7–31 nm in diameter, respectively. In accord with Reference [14], the pore size significantly affects the sorbent characteristics. According to the STA results in Figure 4, the heat flow tends to increase for zeolite 13X and decrease for activated alumina after the impregnation of $MgSO_4$, which indicates that the pore-blocking effect in host matrices with larger pores is severer than that with smaller pores. The reason is that more $MgSO_4$ molecules can be impregnated to the host matrix with larger pores, which obstructs the water adsorption on the pore surfaces to a greater extent. The kinetic hindrance of the hydration of $MgSO_4$ can be solved when the pore sizes are small enough to offer effective dispersion of the salt molecules. However, if the pores are too small, the maximum sorption temperature of the host matrix will be too high for the hydration of $MgSO_4$. Consequently, neither too big or too small pore sizes are recommended. The overall sorption heat diminishes with the increasing pore size of the host matrix due to the decreasing adsorption heat of the host matrix, and meanwhile, the proportion of the hydration heat of $MgSO_4$ rises with the increment of the pore size of the host matrix. There is a trade-off between these influencing factors. Therefore, determination of the optimum host matrix based on the impregnation and reaction mechanism is one of the critical problems in development of composite sorbents.

Sorption TES systems can be sorted into closed systems and open systems according to the cycle types and operation modes. Closed systems, where the heat exchange fluid is separated from the sorbent, have the advantages of better mobility and distributivity. Open systems, where the heat exchange fluid of air has direct contact with the sorbent, generally enjoy higher energy efficiency and better heat and mass transfer performance. Open systems sometimes suffer from the problem of salt and solution leakage along with the outlet air if the salt deliquesces in the sorption process, especially when the salt has low deliquescence relative humidity, such as LiCl and $CaCl_2$. Closed systems do not have the shortcoming of salt and solution leakage, and it can discharge thermal energy to either air or water. According to the experimental results, XM15 is a useful material for closed-system mid-temperature TES due to the high and rapid temperature lift as well as the maximum discharging temperature above 90 °C, which covers the temperature range of both space and water heating. AM16.5 realizes the extended sorption heat release for closed-system low-temperature TES, as the discharging temperature of AM16.5 can be in the range of 40–50 °C for a very long period. For example, at the evaporating temperature of 40 °C, the discharging temperature of AM16.5 is above 47 °C for more than 10 hours. $MgSO_4$ does not radically improve the water uptake capability of the impregnated host matrices. Nevertheless, the high deliquescence relative humidity of $MgSO_4$ can solve the issue of solution leakage for open systems. In consequence, both XM15 and AM16.5 are also useful materials for open-system TES.

6. Conclusions

In this article, the TES performances of the $MgSO_4$-impregnated zeolite 13X and activated alumina are investigated. The following conclusions are made from this study:

(1) The impregnated $MgSO_4$ improves the overall TES performances of both zeolite 13X and activated alumina. The experimental energy storage densities of XM15/ENG-TSA and AM16.5/ENG-TSA are 123.4 kWh m^{-3} and 82.6 kWh m^{-3}, respectively. The temperature lifts of XM15/ENG-TSA and AM16.5/ENG-TSA are 69.2 °C and 16.7 °C, respectively.

(2) Compared to the raw host matrices, the impregnated $MgSO_4$ remarkably accelerates the temperature-rising rate of zeolite 13X to about three times and improves the temperature lift of activated alumina by 32.5%. The sorption temperature region of activated alumina is more aligned with the preferred hydration temperature of $MgSO_4$ in comparison with zeolite 13X.

(3) XM15 is a useful material for closed-system mid-temperature TES with the maximum discharging temperature above 90 °C. AM16.5 realizes the extended sorption heat release for closed-system low-temperature TES of 40–50 °C. The hydration characteristics of $MgSO_4$ can resolve the solution leakage issue of open systems, so both XM15 and AM16.5 are useful materials for open-system TES.

(4) Entransy provides the possibility of assessing thermally and electrically driven TES systems reasonably with the identical thermodynamic evaluation index. Entransy loss and entransy efficiency are useful for assessment of TES systems especially when the exergy difference between charging heat and excess electricity is of marginal importance.

Acknowledgments

This research was supported by the Foundation for Innovative Research Groups of the National Natural Science Foundation of China (Grant No. 51521004) and the International Exchanges 2015 Cost share Programme of the UK's Royal Society (Grant No. IE150678) and the National Natural Science Foundation of China (Grant No. 51611130200).

The first author gratefully acknowledges the financial support by the UK–China Joint Research and Innovation Partnership Fund (known in the UK as the Newton Fund) PhD Placement of the British Council and the China Scholarship Council (Grant No. 201603780099) during the visit to the United Kingdom.

References

[1] Luo M, Wang Z, Brager G, Cao B, Zhu Y. Indoor climate experience, migration, and thermal comfort

expectation in buildings. Building and Environment. 2018;141:262-72.

[2] Transition to Sustainable Buildings: Strategies and Opportunities to 2050: International Energy Agency (IEA), 2013.

[3] Estimates of heat use in the United Kingdom in 2012: Department of Energy & Climate Change, The UK Government, 2013.

[4] Yan T, Li TX, Wang RZ. 18 - Thermochemical heat storage for solar heating and cooling systems. Advances in Solar Heating and Cooling: Woodhead Publishing; 2016. p. 491-522.

[5] The Future of Heating: A strategic framework for low carbon heat in the UK. London, UK: Department of Energy and Climate Change, 2012.

[6] Finck C, Li R, Kramer R, Zeiler W. Quantifying demand flexibility of power-to-heat and thermal energy storage in the control of building heating systems. Applied Energy. 2018;209:409-25.

[7] Lund PD, Lindgren J, Mikkola J, Salpakari J. Review of energy system flexibility measures to enable high levels of variable renewable electricity. Renewable and Sustainable Energy Reviews. 2015;45:785-807.

[8] Aydin D, Casey SP, Riffat S. The latest advancements on thermochemical heat storage systems. Renewable and Sustainable Energy Reviews. 2015;41:356-67.

[9] Tatsidjodoung P, Le Pierrès N, Luo L. A review of potential materials for thermal energy storage in building applications. Renewable and Sustainable Energy Reviews. 2013;18:327-49.

[10] Xu SZ, Lemington, Wang RZ, Wang LW, Zhu J. A zeolite 13X/magnesium sulfate–water sorption thermal energy storage device for domestic heating. Energy Conversion and Management. 2018;171:98-109.

[11] Bales C, Gantenbein P, Jaenig D, Kerskes H, Summer K, van Essen M. Laboratory tests of chemical reactions and prototype sorption storage units. A Report of IEA Solar Heating and Cooling programme – Task 32 Advanced storage concepts for solar and low energy buildings: Report B4 of Subtask B. 2008.

[12] Van Essen V, Bleijendaal L, Kikkert B, Zondag H, Bakker M, Bach P. Development of a compact heat storage system based on salt hydrates. Conference Development of a compact heat storage system based on salt hydrates.

[13] Linnow K, Niermann M, Bonatz D, Posern K, Steiger M. Experimental Studies of the Mechanism and Kinetics of Hydration Reactions. Energy Procedia. 2014;48:394-404.

[14] Posern K, Linnow K, Niermann M, Kaps C, Steiger M. Thermochemical investigation of the water uptake behavior of MgSO4 hydrates in host materials with different pore size. Thermochimica Acta. 2015;611:1-9.

[15] Posern K, Osburg A. Determination of the heat storage performance of thermochemical heat storage materials based on SrCl2 and MgSO4. Journal of Thermal Analysis and Calorimetry. 2018;131(3):2769-73.

[16] Aristov YI. Novel Materials for Adsorptive Heat Pumping and Storage: Screening and Nanotailoring of

Sorption Properties. JOURNAL OF CHEMICAL ENGINEERING OF JAPAN. 2007;40(13):1242-51.

[17] Hongois S, Kuznik F, Stevens P, Roux J-J. Development and characterisation of a new MgSO4−zeolite composite for long-term thermal energy storage. Solar Energy Materials and Solar Cells. 2011;95(7):1831-7.

[18] Xu C, Yu Z, Xie Y, Ren Y, Ye F, Ju X. Study of the hydration behavior of zeolite-MgSO4 composites for long-term heat storage. Applied Thermal Engineering. 2018;129:250-9.

[19] Brancato V, Calabrese L, Palomba V, Frazzica A, Fullana-Puig M, Solé A, et al. MgSO4·7H2O filled macro cellular foams: An innovative composite sorbent for thermo-chemical energy storage applications for solar buildings. Solar Energy. 2018;173:1278-86.

[20] Whiting G, Grondin D, Bennici S, Auroux A. Heats of water sorption studies on zeolite–MgSO4 composites as potential thermochemical heat storage materials. Solar Energy Materials and Solar Cells. 2013;112:112-9.

[21] Mahon D, Claudio G, Eames PC. An experimental investigation to assess the potential of using MgSO4 impregnation and Mg2+ ion exchange to enhance the performance of 13X molecular sieves for interseasonal domestic thermochemical energy storage. Energy Conversion and Management. 2017;150:870-7.

[22] van Essen VM, Cot Gores J, Bleijendaal LPJ, Zondag HA, Schuitema R, Bakker M, et al. Characterization of Salt Hydrates for Compact Seasonal Thermochemical Storage. ASME 2009 3rd International Conference on Energy Sustainability, Volume 2. 2009(48906):825-30.

[23] Shigeishi RA, Langford CH, Hollebone BR. Solar energy storage using chemical potential changes associated with drying of zeolites. Solar Energy. 1979;23(6):489-95.

[24] B. D, E.-H. A, D.-M. G. Experimental investigation of an adsorptive thermal energy storage. International Journal of Energy Research. 2007;31(2):135-47.

[25] van Alebeek R, Scapino L, Beving MAJM, Gaeini M, Rindt CCM, Zondag HA. Investigation of a household-scale open sorption energy storage system based on the zeolite 13X/water reacting pair. Applied Thermal Engineering. 2018;139:325-33.

[26] Tatsidjodoung P, Le Pierrès N, Heintz J, Lagre D, Luo L, Durier F. Experimental and numerical investigations of a zeolite 13X/water reactor for solar heat storage in buildings. Energy Conversion and Management. 2016;108:488-500.

[27] Yu N, Wang RZ, Lu ZS, Wang LW. Development and characterization of silica gel–LiCl composite sorbents for thermal energy storage. Chemical Engineering Science. 2014;111:73-84.

[28] Courbon E, D'Ans P, Permyakova A, Skrylnyk O, Steunou N, Degrez M, et al. Further improvement of the synthesis of silica gel and CaCl2 composites: Enhancement of energy storage density and stability over cycles for solar heat storage coupled with space heating applications. Solar Energy. 2017;157:532-41.

[29] Zhao YJ, Wang RZ, Zhang YN, Yu N. Development of SrBr2 composite sorbents for a sorption thermal energy storage system to store low-temperature heat. Energy. 2016;115:129-39.

[30] Cabeza LF, Solé A, Barreneche C. Review on sorption materials and technologies for heat pumps and thermal energy storage. Renewable Energy. 2017;110:3-39.

[31] Wang LW, Wang RZ, Oliveira RG. A review on adsorption working pairs for refrigeration. Renewable and Sustainable Energy Reviews. 2009;13(3):518-34.

[32] Zhang YN, Wang RZ, Zhao YJ, Li TX, Riffat SB, Wajid NM. Development and thermochemical characterizations of vermiculite/SrBr2 composite sorbents for low-temperature heat storage. Energy. 2016;115:120-8.

[33] Grekova AD, Gordeeva LG, Aristov YI. Composite "LiCl/vermiculite" as advanced water sorbent for thermal energy storage. Applied Thermal Engineering. 2017;124:1401-8.

[34] Casey SP, Aydin D, Riffat S, Elvins J. Salt impregnated desiccant matrices for 'open' thermochemical energy storage—Hygrothermal cyclic behaviour and energetic analysis by physical experimentation. Energy and Buildings. 2015;92:128-39.

[35] Zhang YN, Wang RZ, Li TX. Thermochemical characterizations of high-stable activated alumina/LiCl composites with multistage sorption process for thermal storage. Energy. 2018;156:240-9.

[36] Zhang YN, Wang RZ, Li TX. Experimental investigation on an open sorption thermal storage system for space heating. Energy. 2017;141:2421-33.

[37] Jiang L, Roskilly AP, Wang RZ, Wang LW, Lu YJ. Analysis on innovative modular sorption and resorption thermal cell for cold and heat cogeneration. Applied Energy. 2017;204:767-79.

[38] Jiang L, Gao J, Wang L, Wang R, Lu Y, Roskilly AP. Investigation on performance of multi-salt composite sorbents for multilevel sorption thermal energy storage. Applied Energy. 2017;190:1029-38.

[39] Xu SZ, Wang RZ, Wang LW. Temperature–heat diagram analysis method for heat recovery physical adsorption refrigeration cycle – Taking multi-stage cycle as an example. International Journal of Refrigeration. 2017;74:254-68.

[40] Zhao Y, You Y, Liu HB, Zhao CY, Xu ZG. Experimental study on the thermodynamic performance of cascaded latent heat storage in the heat charging process. Energy. 2018;157:690-706.

[41] Zheng Z-J, He Y, He Y-L. Optimization for a Thermochemical Energy Storage-reactor based on Entransy Dissipation Minimization. Energy Procedia. 2015;75:1791-6.

[42] Xu SZ, Wang RZ, Wang LW. Reply and closure to comments on "Temperature–heat diagram analysis method for heat recovery physical adsorption refrigeration cycle – Taking multi-stage cycle as an example" by M.M. Awad. International Journal of Refrigeration. 2017;82:543-7.